

Mechanisms of genuine humic acid evolution and its dynamic interaction with methane production in anaerobic digestion processes

Xiqing Wang¹, Atif Muhmood¹, Tao Lyu², Renjie Dong¹, Hongtao Liu³, Shubiao Wu^{*4}

¹Key Laboratory of Clean Utilization Technology for Renewable Energy, Ministry of Agriculture, College of Engineering, China Agricultural University, 100083, Beijing, P. R. China

²Cranfield Water Science Institute, Cranfield University, College Road, Cranfield, Bedfordshire, MK43 0AL, UK

³Institute of Geographic Science and Natural Resources Research, Chinese Academy of Sciences, Beijing 100101, China

⁴Aarhus Institute of Advanced Studies, Aarhus University, DK-8000 Aarhus C, Denmark

*Correspondence. E-mail: wushubiao@gmail.com

Abstract

Humic acid (HA), a byproduct formed during the biological conversion of organic matter into biogas in the anaerobic digestion (AD) process, contains complex structures and redox functions. However, the evolution mechanism of HA and its interaction with CH₄ production during the AD process have not been fully explored, particularly with respect to various substrates and temperature conditions. In this study, we investigated the evolutionary dynamics of the structure and function of genuine HA that naturally formed in the AD processes of chicken manure and corn stover under mesophilic (37 °C) and thermophilic (55 °C) conditions. The results demonstrated that the HA evolution mechanisms in AD of chicken manure and corn stover have different pathways. The AD of core stover showed higher degree of aromaticity (41.2-66.7% and 45.3-68.4% for mesophilic and thermophilic respectively) and humification index (1.5-4.2 and 2.8-4.5 for mesophilic and thermophilic respectively) than those (28.3-45.3% and 30.2-54.5% of aromaticity and 0.6-1.2 and 1.3-3.7 of humification index) in AD of chicken manure. The

24 results from HSQC NMR spectroscopy and 2D-COS-FTIR spectroscopy demonstrated an
25 accelerating effect of the higher temperature on the evolution of HA through
26 humification. Moreover, the concurrent decomposition and re-polymerization of HA
27 during both AD processes, resulting in positive and negative effects on CH₄ production
28 in the fast and slow CH₄ production stages, respectively. The dynamic interaction was
29 due to variations in the electron transferring ability and structure of the formed HA. The
30 results could not only advance our understanding of the mechanisms of HA evolution
31 and its interaction with the performance of AD process, but also support further
32 research toward improving AD performance by regulating HA formation and
33 transformation.

34 **Keywords:** Biogas production; humic substances; humification; redox capacity; re-
35 polymerization

36 **1. Introduction**

37 Anaerobic digestion (AD) is a widely implemented biological technology in agriculture
38 that not only offers an appropriate treatment of various agricultural residuals but also
39 provides essential, clean, and affordable renewable energy to society ([Maynaud et al.,](#)
40 [2017](#); [Somers et al., 2018](#)). In AD processes, organic matter is degraded via a series of
41 microbially mediated reactions initiated by hydrolysis of organic macromolecules into
42 soluble organic units, followed by the production of CH₄ and CO₂ by degrading these
43 soluble compounds via the pathways of acidogenesis, acetogenesis, and
44 methanogenesis ([Martins das Neves et al., 2009](#); [Sepehr et al., 2018](#)). The occurrence of
45 these biological degradations leads to the production of a great variety of organic

46 components such as polyphenols and polysaccharides that can form recalcitrant
47 macromolecular organics, such as humic substances (HS), through the re-polymerization
48 process (Sánchez-Monedero et al., 1999; Baddi et al., 2009). Thus, humic acid (HA), as a
49 major fraction of HS has shown to be a bulk component and usually accounts for 10–20%
50 of the total solids in the anaerobic digesters, with 5–10 g/L of content, which varies
51 depending on the feeding materials and operational conditions (Yap et al., 2018; Guo et
52 al., 2019).

53 The HA has been deemed a complicated macromolecule that contains many active
54 functional groups, such as carboxylic acid, phenolic, and quinone types (Said-Pullicino et
55 al., 2016; Nie et al., 2018). Recently, the impact of HA on AD performance has
56 increasingly attracted the attention of scientists, and some laboratory experiments have
57 been conducted to study the interaction through the addition of commercial HA or HA
58 analogs in the AD process (Yap et al., 2017; Li et al., 2019a; Bai et al., 2019). The main
59 mechanistic hypothesis concluded from these investigations on the inhibiting impact of
60 HA on the AD performance is due to the binding of active functional groups in HA to the
61 active sites of relevant key enzymes (such as hydrolytic enzymes), thereby preventing
62 their access to substrates (Yap et al., 2017). Moreover, HA has recently been reported
63 to serve as terminal electron acceptors during microbial respiration and function as
64 electron shuttles driving the anaerobic oxidation of methane (Bai et al., 2019) and
65 accelerating the consumption of organic substances during the AD process (Wang et al.,
66 2019). Although a few recent studies have observed the inhibiting effect of commercial
67 HA on the AD process, which is indicated by the reduced CH₄ production, the conclusions
68 may hardly be applied to understand the impact of genuine HA that naturally forms in

69 the AD process (Yap et al., 2017 and 2018; Li et al., 2019b). The structure and function
70 of the commercial HA are relatively consistent during the whole AD experiment, which
71 is insufficient to be representative of the naturally formed HA with dynamic abundance,
72 active functional groups, and electron transferring abilities in different phases of the AD
73 process (Tang et al., 2018; Ma et al., 2019). Therefore, *in-situ* monitoring of naturally
74 formed HA with dynamic characteristics is crucial for re-evaluating and understanding
75 the underlying mechanisms of the effect of HA on AD performance.

76 The process of HA formation, also called humification, involves various microorganism-
77 dominated biological and biochemical processes (Hayes et al., 2009; Mylotte et al.,
78 2016). To date, different hypotheses, including lignin-protein theory, polyphenol theory,
79 and sugar-amine condensation theory, have been used to explain the humification (Tan,
80 2014; Wu et al., 2017; Gao et al., 2019). Generally, the complex organic compounds
81 containing HA precursors could first be decomposed into small-molecule organics and
82 then transformed into recalcitrant macromolecular organic products through the
83 repolymerization to form HA under relevant microorganism functions (Gao et al., 2019).
84 For example, Tang et al. (2020) found the original HA in extracellular polymeric
85 substances could be degraded and modified, and HA with abundant aromatic sites may
86 also bridge protein condensation to regenerate HA during sewage sludge AD process
87 (Tang et al., 2020). Moreover, during humification, precursors from different sources
88 (feeding materials in the AD process) would enable the formation of HA with different
89 molecular compositions, structures, and functionalities due to the different elemental
90 compositions and properties of raw materials (Sale et al., 2015; He et al., 2018). Likewise,
91 the fermentation temperature could also affect the humification pathway and the

92 stability of the formed HA (Jiang et al., 2015; Onwosi et al., 2017). Nevertheless, current
93 knowledge about HA formation mechanisms is largely derived from research on
94 composting, which is primarily led by a group of aerobic microorganisms (Gao et al.,
95 2019; He et al., 2015). Although the phenomenon of HA formation has been observed
96 in the anaerobic digestion (Tang et al., 2018; Tang et al., 2020), the evolutionary
97 dynamics of HA in the AD process, which is dominated by anaerobic microorganisms,
98 have not yet been fully understood (Appels et al., 2008), particularly under conditions
99 with varying feeding materials and operating temperatures. Moreover, information on
100 the dynamics of active functional groups and the electron transferring ability of the
101 naturally formed HA in the entire AD process and its interaction with CH₄ production is
102 insufficient.

103 To address this knowledge gap, we investigated the evolutionary dynamics of genuine
104 HA and its interaction with CH₄ production during different stages of AD processes with
105 two feeding materials, chicken manure and corn stover, under mesophilic (37 °C) and
106 thermophilic (55 °C) conditions. In addition to HA abundance, changes in the structure
107 and active functional groups of HA were determined by two-dimensional correlation
108 (2D-COS) of a Fourier transform infrared spectra (FTIR) and one-bond ¹H–¹³C
109 heteronuclear single quantum coherence (HSQC) nuclear magnetic resonance (NMR)
110 spectra. The dynamics of the electron transfer capability of HA was detected to elucidate
111 its potential effect on CH₄ generation. Moreover, structural equation modeling (SEM)
112 and principal component analysis (PCA) combined with the results from pyrolysis–gas
113 chromatography/mass spectroscopy (Py-GC/MS) were conducted to reveal the
114 underlying HA evolution mechanisms and their interactions with CH₄ production.

115 **2. Materials and methods**

116 **2.1 Setup of the batch AD experiments**

117 Batch AD experiments were conducted in this study using 120 mL serum bottles with a
118 working volume of 60 mL. The commonly used AD feeding materials (chicken manure
119 and corn stover) were fermented under mesophilic (37 °C) and thermophilic (55 °C)
120 conditions for 40 days. The chicken manure was collected from the Deqingyuan biogas
121 plant, which is located in the suburbs of Beijing, China. The total solid (TS) and volatile
122 solid (VS) contents of the chicken manure were 10.01% and 7.88%, respectively (Table
123 1). The corn stover was obtained from the University farm of China Agricultural
124 University in Beijing, China, and had TS and VS values of 85.90% and 73.12%, respectively
125 (Table 1). Likewise, the sludge from long-term laboratory-scale mesophilic (37 °C)
126 digesters fed with chicken manure (TS of 4.98% and VS of 2.23%) and corn stover (TS of
127 6.75% and VS of 3.45%) were used as the corresponding inoculum for the AD of chicken
128 manure and corn stover, respectively. Moreover, the sludge from long-term laboratory-
129 scale mesophilic (55 °C) digesters fed with chicken manure (TS of 5.01% and VS of 1.98%)
130 and corn stover (TS of 6.52% and VS of 3.05%) were used as the corresponding inoculum
131 for the AD of chicken manure and corn stover, respectively. The organic matter ratio of
132 the substrate and the inoculum was 1:2 (Guo et al., 2018). The experimental AD bottles
133 were marked and placed in a temperature-controlled incubator (RZH-380A, artificial
134 climate chamber, China), and each treatment was performed in triplicate. Four replicate
135 bottles filled with inoculum alone were used as blanks in each treatment group under
136 the same experimental conditions. Further details on the setup of the batch
137 experiments can be found in Text S1 of the Supporting Information.

138
139

Table 1
Characteristic of chicken manure, corn stover and inoculum sludge

Parameters	pH	TS (%)	VS (%)	VS/TS (%)
Chicken manure	7.52±0.20	10.01±0.50	7.88±0.41	78.72±0.32
Corn stover	/	85.90±0.45	73.12±0.38	85.10±0.61
Inoculum sludge (Chicken manure, 37°C)	7.89±0.09	4.98±0.25	2.23±0.17	44.78±0.43
Inoculum sludge (Chicken manure, 55°C)	7.95±0.12	5.01±0.31	1.98±0.26	39.52±0.52
Inoculum sludge (Corn stover, 37°C)	7.22±0.11	6.75±0.18	3.45±0.14	51.11±0.29
Inoculum sludge (Corn stover, 55°C)	7.19±0.13	6.52±0.16	3.05±0.11	46.78±0.12

140 Daily biogas production was measured using a water displacement manometer (GF-500,
141 KIMO, France). The biogas composition was analysed via gas chromatography with a
142 thermal conductivity detector (SP 2100, BFRL, China). The Gompertz model was used to
143 fit the measured CH₄ yield and identify two CH₄ production stages (fast and slow) (Zhang
144 et al., 2014). The digested slurry was regularly sampled every five days and then
145 immediately analysed in the laboratory for physicochemical properties, including pH,
146 total solids, and volatile solids (VS), according to the standard methods (APHA, 1998;
147 Luo et al., 2018). Further details on the analysis of these physicochemical properties are
148 described in Text S2-1 of the Supporting Information.

149 **2.2 Characteristics of fluorescent components**

150 The excitation–emission matrix (EEM) spectra were recorded using a fluorescence
151 spectrophotometer (Aqualog, HORIBA) to analyze the evolution of the OM in the AD
152 process. The sampled digested slurry was first diluted with distilled water 50 times

153 before the fluorescence spectra analysis. The emission wavelengths (250–550 nm) and
154 excitation wavelengths (250–600 nm) over the range were observed in 5 and 3 nm
155 increments, respectively. The Rayleigh and Raman scattering of the EEM data were
156 calibrated using the method described by [Bahram et al. \(2006\)](#). Finally, parallel factor
157 (PARAFAC) analysis was carried out using MATLAB R2018a (MathWorks, USA) with the
158 DOMFluor Toolbox. Moreover, the fluorescence parameters, including biological index
159 (BIX) and humification index (HIX), were obtained using the data collected through
160 fluorescence spectroscopy. Further detailed information on the EEM and PARAFAC
161 analyses are described in Text S2-2 of the Supporting Information.

162 **2.3 Extraction of humic acid in the sampled digested slurry**

163 The extraction and purification of the HA fraction in the sampled digested slurry were
164 conducted according to the standard method recommended by the International Humic
165 Substances Society ([Swift et al., 1996](#)). Briefly, the sampled digested slurry was first
166 shaken (200 rpm, 24 h) with a mixed solution of 0.1 M $\text{Na}_4\text{P}_2\text{O}_7$ and 0.1 M NaOH at a
167 1:10 (w:v) ratio at room temperature. The supernatant was filtered through a 0.45 μm
168 Millipore membrane after 20 min of centrifugation (11,000 rpm). The procedure was
169 repeated three times, and the supernatant was filtered through a 0.45 μm Millipore
170 membrane, acidified with 6 M HCl to pH 1 and left overnight. The precipitate was
171 separated from the liquid phase by centrifugation (5000 rpm, 10 min), suspended in 100
172 ml NaOH and $\text{Na}_4\text{P}_2\text{O}_7$ mixed solution and shaken overnight. The solution was then
173 centrifuged (5000 rpm, 10 min), and the liquid phase was acidified with 0.1 M HCl/0.3
174 M hydrogen fluoride to pH 1, left to stand overnight and centrifuged. The precipitated

175 was dialyzed against distilled water until Cl⁻ could no longer be detected (Zhao et al.,
176 2020).

177 **2.4 Humic acid characterization**

178 The carbon (C), hydrogen (H), and nitrogen (N) contents of HA were analysed using an
179 elemental analyzer (Vario EL cube, Germany); the H/C, C/N, and C/O ratios were
180 calculated to analyse the elemental characteristics of HAs. The parameter-specific UV
181 absorbance at 254 nm and 280 nm was measured using a UV-vis spectrophotometer
182 (Shimadzu, UV-2600). SUVA₂₅₄ is used to characterize the relative aromaticity of HA
183 (Weishaar et al., 2003); similarly, SUVA₂₈₀ is suitable for tracking the π - π^* electron
184 transitions in the UV range (270–280 nm) for phenolic substances, aniline derivatives,
185 benzoic acids, polyenes, and polycyclic aromatic hydrocarbons (Tang et al., 2018). The
186 content changes in the aliphatic and aromatic components of HA were complemented
187 by one-bond ¹H–¹³C HSQC NMR spectra using an Avance III 600 MHz spectrometer
188 (Bruker, The Woodlands, TX). Detailed information on this method is described in Text
189 S2-3 (Supporting Information).

190 FTIR spectra, a mainstream tool for determining functional groups and analyzing the
191 structural composition of sampled HA, was utilized in this study using a Nicolet IS10 FTIR
192 spectrophotometer from 4,000 to 400 cm⁻¹ (Zhou et al., 2014). Then, two-dimensional
193 correlation spectra (2D-COS) were used to improve the spectral resolution and
194 characterize the changing degree and order of different functional groups under
195 different conditions. The interpretation of the synchronous and asynchronous plots
196 obtained from 2D-COS was mainly based on Noda's rule (Noda and Ozaki, 2004);
197 additional details are provided in Text S2-4 (Supporting Information).

198 To further investigate the qualitative characterization of the molecular composition of
199 the extracted HA in this study, pyrolysis–gas chromatography/mass spectroscopy (Py-
200 GC/MS) analysis was performed on a Pyroprobe pyrolyzer (6890 GC/5973 MSD, Agilent,
201 USA). Py-GC/MS analysis for each sample was repeated twice and found to have proper
202 repeatability. The compounds obtained through GC/MS were identified via the NIST
203 database by closest match in the NIST MS Search 2.3 using identity-type searching. The
204 threshold for the match factor was 85% (Shahbeig and Nosrati, 2020). The detailed
205 information can be found in Text S2-5 (Supporting Information).

206 To explore the potential of HA to serve as terminal electron acceptors during microbial
207 respiration and function as electron shuttles to drive the redox bioconversion of organic
208 molecules in the AD process (Tan et al., 2017), the electron transfer capacities (ETCs),
209 including the electron-donating capacity (EDC) and electron-accepting capacity (EAC) of
210 HA, were measured using mediated electrochemical reduction and oxidation methods
211 (Wang et al., 2020). Detailed information on this method is described in Text S2-6
212 (Supporting Information).

213 **2.5 Principal component analysis and structural equation modelling**

214 PCA was used to identify different AD performance patterns during the entire AD
215 process at different temperatures. The components used for PCA included CH₄
216 production, HIX, and all the OM components during the AD process of chicken manure
217 and corn stover. A cluster analysis was performed according to the eigenvalues of each
218 component, and the results were used to group similar patterns in the PCA coordinates.
219 SEM was then used to clarify the direct and indirect relationships between HA formation
220 and its impact on the AD process (Gao et al., 2019). Before SEM analysis, auto-regressive

221 correlation structures were used to identify potential autocorrelations in the IBM SPSS
222 AMOS 23.0 data. Then, we established an *a priori* model according to our current
223 knowledge of HA formation and interaction with CH₄ production, and the data matrix
224 was fitted to the model using the maximum-likelihood estimation method with AMOS
225 23.0 software (SPSS Inc., Chicago, IL). The χ -square test in SPSS software was used to
226 verify the quality of the fit. Finally, we determined the structural changes of HA and the
227 factors affecting CH₄ production, and we calculated the weight of each factor's influence
228 on CH₄ production.

229 **3. Results and discussion**

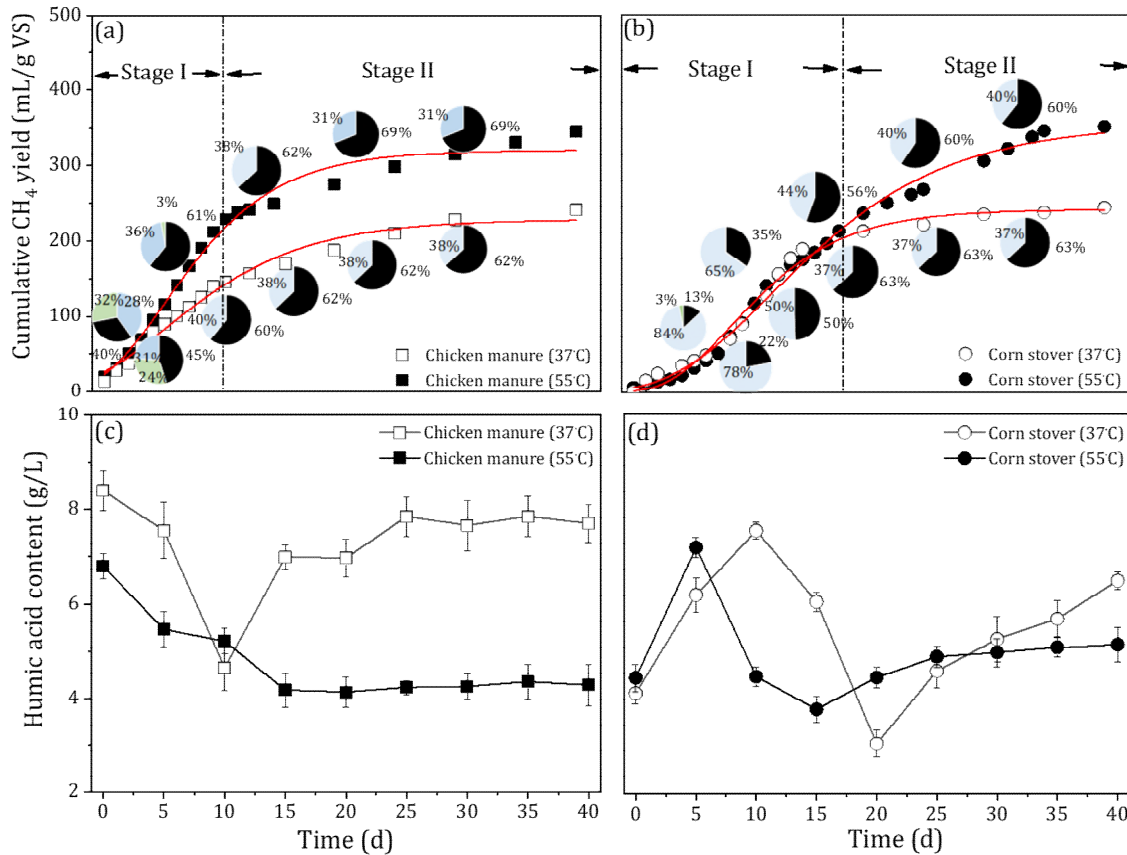
230 **3.1 Organic matter transformation in the AD process**

231 During the mesophilic AD process, approximately 12% and 2% of the cumulative CH₄
232 yields of chicken manure and corn stover (254±7 and 227±6 mL gVS⁻¹, respectively) were
233 lower than the yields obtained in the thermophilic AD process (327±9 and 321±10 mL
234 gVS⁻¹, respectively) (Fig. 1a and b). CH₄ generation in AD was mainly achieved by the
235 microbially mediated transformation of the organics ([Martins das Neves et al., 2009](#);
236 [Sepehr et al., 2018](#)), and higher temperature fermentation conditions had the
237 advantage of increasing the hydrolysis rate of organics toward increased CH₄ production
238 ([Croce et al., 2016](#)). These results were also supported by the higher degradation of VS
239 in the thermophilic AD process (39.6% and 39.6% for chicken manure and corn stover,
240 respectively) than those in the mesophilic AD process (38.3% and 34.8% for chicken
241 manure and corn stover, respectively) (Table S1 and S2). Along with the AD process, the
242 CH₄ production rate is strongly replied on the microbial degradation rate of the organic
243 matter. Based on this concept, the Gompertz model, as a classical kinetic model, has

244 been developed to simulate the CH₄ production and distinguish different stages of the
245 CH₄ production rates in AD process (Zhang et al., 2014). According to the determined
246 daily CH₄ generation (Fig. S1) and the theoretical Gompertz model, the transmission of
247 fast (stage I, Fig. 1) and slow (stage II, Fig. 1) CH₄ production stages were identified for
248 the AD of chicken manure (day 10) and corn stover (day 18) without differences between
249 the mesophilic and thermophilic conditions.

250 PARAFAC analyses based on the EEM fluorescence spectra were used to illustrate the
251 transformations of OM in the AD process (Fig. 2a–h). Five fluorescent components were
252 identified (Table S3), comprising two humic-like compounds (C1 and C3), one fulvic-like
253 compound (C2), protein-like and tyrosine-like substances (C4), and tryptophan-like
254 substances (C5) (He et al., 2015; Wang et al., 2020). Among them, the abundance of
255 protein-like components decreased with an increase in the humic-like components
256 during the AD process for both materials (Fig. S2). Along with the transformation of OM,
257 the content of HA decreased from 8.4 ± 0.9 to 4.6 ± 0.6 g L⁻¹ in the fast CH₄ production
258 stage and then gradually increased to 7.7 ± 0.8 g L⁻¹ during the slow CH₄ production
259 stage of the mesophilic AD of chicken manure (Fig. 1c). However, under the thermophilic
260 conditions, the content of HA continuously decreased from the initial value of 6.8 ± 0.7
261 to 4.1 ± 0.4 g L⁻¹ in the fast CH₄ production stage and maintained a similar level until the
262 end of the experiment. The dynamics of the HA content in the AD of corn stover showed
263 a different tendency (Fig. 1d). The HA content increased from 4.5–4.9 to 7.1–7.5 g L⁻¹ in
264 the first five days and then decreased to 3.9–4.1. g L⁻¹ in the fast CH₄ production stage
265 under both temperature conditions. In the slow CH₄ production stage, the HA content
266 gradually increased to 4.6–5.2. g L⁻¹ by day 40.

267 Integrating the dynamics of HA content during the AD process (Fig. 1c and d) indicated
268 the concurrent decomposition and formation of HA during the AD process. It was
269 reported that the initial HA content in the feeding material and/or inoculum would first
270 degrade in the fast CH₄ production stage along with the biodegradation of the organics
271 ([Tang et al., 2018](#)); however, in the following slow CH₄ generation stage, essential
272 precursors to the formation of HA, such as polyphenols, carboxylic acids, and amino
273 acids via the transformation of the OM, could be generated and lead the re-
274 polymerization of HA ([Gao et al., 2019](#)). Notably, the fast HA content increase in the
275 early stage for corn stover (Fig. 1d) may be attributed to the abundance of fiber-
276 structural components (e.g., lignin), which provides more stable phenolic compounds
277 required as starting materials for humification processes ([Lopez et al., 2002](#)). Moreover,
278 significantly lower HA contents were quantified under the thermophilic conditions than
279 in the mesophilic conditions, indicating the stimulating effect of higher temperatures on
280 HA degradation ([Putranto et al., 2017](#)). This can be attributed to the faster microbial
281 degradation of polysaccharides, proteins, and fats to CH₄ instead of re-polymerization
282 to HA ([Jiang et al., 2015](#); [Onwosi et al., 2017](#)), which results in higher biogas production
283 under the thermophilic AD process (Fig. 1a and b).



284

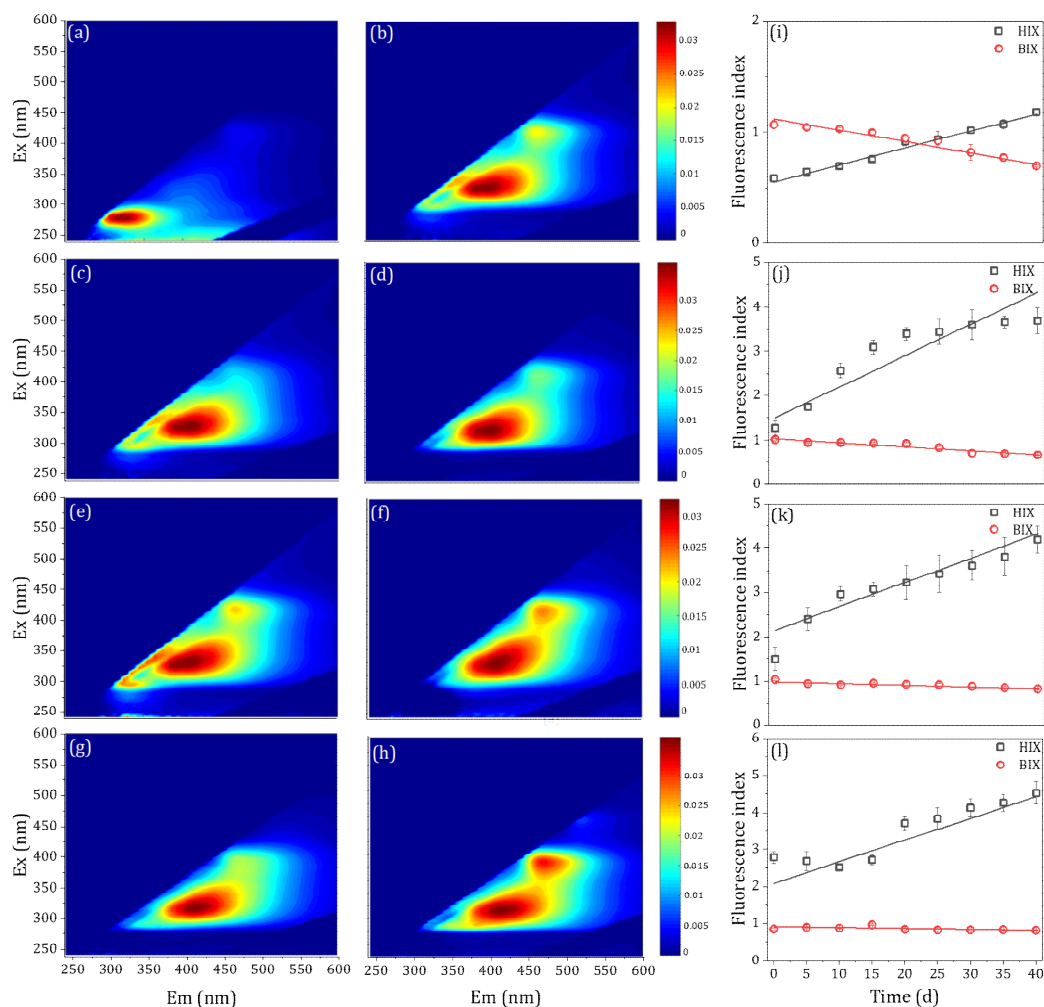
285 **Fig. 1.** The cumulative methane produced and humic acid content during chicken manure (a, c)
 286 and corn stover (b, d) anaerobic digestion at different temperatures. The black, blue, and green
 287 areas in the pie chart represent methane, carbon dioxide, and nitrogen content, respectively
 288 (Stage I: fast methane production stage; Stage II: Slow methane production stage).

289 3.2 Characterization of the humification process

290 Target fluorescence indexes, including biological index (BIX) and humification index
 291 (HIX), were calculated to evaluate the characteristics of the humification process for HA
 292 formation in different AD processes (Fig. 2i–l). BIX is commonly used to evaluate the
 293 autochthonous biological activity of the formed HA, where a high BIX value corresponds
 294 to the presence of freshly produced HA (Tedetti et al., 2011; He et al., 2015). In this study,
 295 the declining trend of the BIX value in both AD processes of chicken manure (from 1.01–
 296 1.06 to 0.65–0.69) and corn stover (from 0.95–1.03 to 0.81–0.82) represented the aging
 297 process of the freshly formed HA to the humified structure. Besides, HIX is a general

298 indicator of the degree of humification of HA and is positively related to the complexity
299 of the structure (Huguest et al., 2009). The HIX values of the formed HA in the
300 thermophilic AD process (1.26–3.68) were significantly higher than those in the
301 mesophilic AD of chicken manure (0.58–1.18), indicating the positive effect of higher
302 temperature on the HA humification process (Fig. 1c) (Guo et al., 2019).

303 Although the temperature effect on HIX in the AD of corn stover was not significant, the
304 continually increased values (from 1.49–2.77 to 4.19–4.52) indicated the strengthened
305 humification process during the AD process under both temperature conditions (Fig. 2k
306 and l). The influence of temperature on HIX formation is different for distinct substrates
307 may due to the composition of the corn stover has abundant lignocellulosic compounds
308 compared with chicken manure (Gao et al., 2019). To confirm these changes in the
309 structure of HA, the levels of the aromaticity of HA in different AD processes were
310 further determined by HSQC NMR spectroscopy (Fig. S3). Similarly, the results showed
311 a higher increase in the aromaticity (30.2–68.4%) in the HA formed in the thermophilic
312 AD process than those (28.3–66.7%) in the mesophilic AD process (Table S4), which
313 agreed with the changes in BIX and HIX. The degradation of superficial labile aliphatics
314 in HA was improved under thermophilic conditions, which might be the reason for the
315 increase in the degree of humification during the thermophilic AD process (Tang et al.,
316 2018).



317

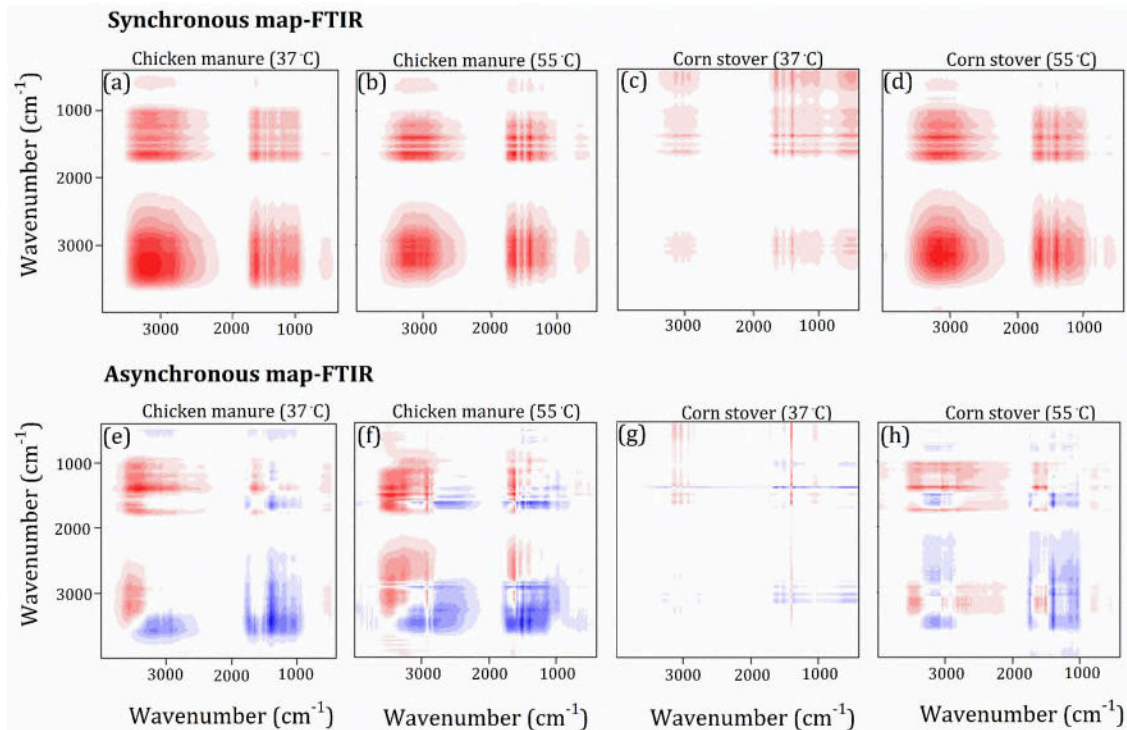
318 **Fig. 2.** Excitation–emission matrix fluorescence spectra of OM, and the humification index (HIX)
 319 and biological index (BIX) evolution during the mesophilic and thermophilic anaerobic digestion of
 320 chicken manure and corn stover. (a, b) mesophilic anaerobic digestion of chicken manure at 0 and
 321 40 days; (c, d) thermophilic anaerobic digestion of chicken manure at 0 and 40 days; (e, f) mesophilic
 322 anaerobic digestion of corn stover at 0 and 40 days; (g, h) thermophilic anaerobic digestion of corn
 323 stover at 0 and 40 days; (i, j) HIX and BIX from the mesophilic and thermophilic anaerobic digestion
 324 of chicken manure, respectively; (k, l) HIX and BIX from the mesophilic and thermophilic anaerobic
 325 digestion of corn stover, respectively.

326 3.3 Variation in the functional groups of HA

327 Due to the complex structure of HA, the simple FTIR image (Fig. S4) cannot identify the
 328 changes in the functional groups based on the obtained infrared absorption spectra
 329 (Gao et al., 2019). Thus, a further 2D-COS analysis was applied to examine the structural
 330 changes in the active functional groups of HA (Fig. 3). In the synchronous 2D-COS IR

331 spectra, a total of six auto-peaks (at 3000, 3400, 1850, 1700, 1230, and 1030 cm^{-1}) and
332 six positive cross-peaks at (1030, 3000), (1700, 3000), (1030, 1850), (1230, 1700), (1700,
333 1850), and (1850, 3000) were determined, and no significant difference between the
334 mesophilic and thermophilic AD of chicken manure and corn stover was observed (Fig.
335 3a–d). Notably, the intensity of the auto-peaks in the 2D-COS IR spectra for HA formed
336 from the mesophilic AD process was lower than that from the thermophilic AD process.
337 Compared with the synchronous maps, the asynchronous 2D-COS analyses of HA
338 formed from the chicken manure and corn stover AD processes showed significant
339 differences, with only cross-peaks detected (Fig. 3e–h). The asynchronous map of HA
340 produced during the AD (mesophilic and thermophilic) of chicken manure contained
341 seven negative cross-peaks at (1030, 3400), (1600, 3400), (2800, 3400), (1230, 3400),
342 (1030, 1700), (1230, 1700), and (1850, 3400), and two positive cross-peaks at (1600,
343 1700) and (1600, 2800). Unlike the chicken manure, three positive cross-peaks at (1600,
344 3000), (1600, 1700), and (2800, 3000) and five negative cross-peaks at (1850, 3000),
345 (1230, 3000), (1030, 1600), (1230, 1600), and (3000, 3400) were observed for HA formed
346 during the (mesophilic and thermophilic) AD of corn stover. According to Noda's rules
347 (Noda and Ozaki, 2004), the peaks reacted in the following order: $2800 \text{ cm}^{-1} > 3400 \text{ cm}^{-1} >$
348 $1700 \text{ cm}^{-1} > 1030 \text{ cm}^{-1}$, $1230 \text{ cm}^{-1} > 1600 \text{ cm}^{-1}$, 1850 cm^{-1} for the AD of chicken manure,
349 and $3400 \text{ cm}^{-1} > 2800 \text{ cm}^{-1} > 1850 \text{ cm}^{-1}$, $1600 \text{ cm}^{-1} > 1700 \text{ cm}^{-1} > 1230 \text{ cm}^{-1}$, 1030 cm^{-1}
350 for the AD of corn stover. Therefore, the active functional groups of HA formed in the
351 chicken manure AD process changed in the sequence of aliphatic-like substances (C-H) >
352 amides (H-N) or carbohydrates (O-H) > carboxylic acids (C=O) > polysaccharides (C=O),
353 phenol > aromatic compounds, ketones (C=C). The active functional groups of HA

354 formed in the corn stover AD process changed in the following sequence: amides (H-N)
355 or carbohydrates (O-H) > aliphatic-like substances (C-H) > aromatic compounds and
356 ketones (C=C) > carboxylic acids (C=O) > polysaccharides (C=O), phenolics (Gao et al.,
357 2019; Yang et al., 2019).



358 **Fig. 3.** 2D-FTIR correlation maps generated from the 400–4000 cm^{-1} region of the spectra of
359 humic acid in the anaerobic digestion of chicken manure and corn stover at different
360 temperatures. Red and blue represent positive and negative correlations, respectively. A more
361 intense color indicates a stronger correlation.
362

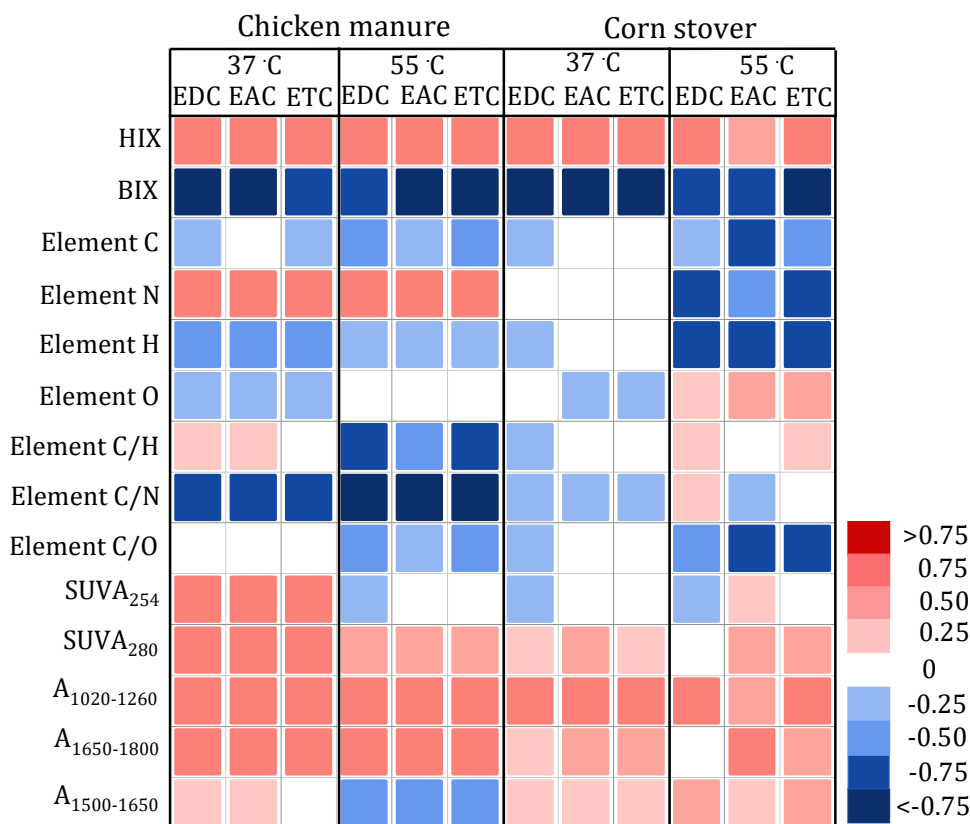
363 3.4 Redox capability evolution of HA

364 The redox capabilities of the HA transformed during the AD of chicken manure and corn
365 stover were assessed by the ETCs of HA (Fig. S5), including the EAC and EDC. The ETCs
366 (both EAC and EDC) of HA increased during the mesophilic and thermophilic AD of
367 chicken manure and corn stover, which indicated the increased capability of the formed
368 HA to influence the microbially mediated organics transformation process (Tan et al.,
369 2017; Zhao et al., 2020). Moreover, both feeding materials and fermentation

370 temperatures significantly affect the redox capability evolution of HA. The ETC values of
371 HA during the mesophilic AD of chicken manure (671 ± 15 – $1469 \pm 23 \mu\text{mol gHA}^{-1}$) and
372 corn stover (687 ± 20 – $1294 \pm 25 \mu\text{mol gHA}^{-1}$) were lower than those (774 ± 22 – $1515 \pm$
373 $18 \mu\text{mol gHA}^{-1}$ and 1013 ± 19 – $1424 \pm 21 \mu\text{mol gHA}^{-1}$ for chicken manure and corn stover,
374 respectively) in the thermophilic AD processes. The results indicated that higher
375 temperatures could facilitate an increase in the ETCs of HA (Tan et al., 2017).

376 The ETCs of HA could contribute to the microbially mediated reactions in the AD process
377 and influence organic transformation and CH_4 generation (Bai et al., 2019). Such redox
378 capacity heavily depends on the structure/composition of HA, such as basic elements (C,
379 N, H, and O) and their ratios (C/H, C/N, and C/O), relative aromaticity (SUVA_{254}), π - π^*
380 electron transitions (SUVA_{280}), functional groups from FTIR detections, and humification
381 degree (HIX and BIX). Thus, Pearson correlation analysis was conducted to evaluate the
382 influence of the characteristics (Table S5, S6, and S7) on the redox capacity of HA for
383 both feeding materials under different temperature conditions (Fig. 4). During the AD of
384 chicken manure, the ETC (EAC and EDC) was positively related to the HIX, element N,
385 SUVA_{254} , SUVA_{280} , carbonyl group, carboxyl group, and ketone group and was negatively
386 correlated with the BIX and C/N ratio. Compared with the chicken manure AD process,
387 only the HIX, carbonyl group, and carboxyl group were positively correlated with the ETC
388 of HA during corn stover AD processes. The obvious effect of the two feeding materials
389 was addressed, which may be due to the distinct organic sources for the AD process (He
390 et al., 2014).

391



392

393 **Fig. 4.** Correlation between the chemical structure and redox properties of humic acid derived
 394 from chicken manure and corn stover anaerobic digestion. (EDC: Electron-donating capacity;
 395 EAC: Electron-accepting capacity; ETC: Electron transfer capacity; HIX: Humification index; BIX:
 396 Biological index; A₁₀₂₀₋₁₂₆₀: The area of 1020–1260 cm⁻¹ from FTIR represents the oxygen-
 397 containing groups (such as the carbonyl group and carboxyl group); A₁₆₅₀₋₁₈₀₀: The area of 1650–
 398 1800 cm⁻¹ from FTIR represents the ketone groups; A₁₅₀₀₋₁₆₅₀: The area of 1500–1650 cm⁻¹ from
 399 FTIR represents the N-H and amide groups)

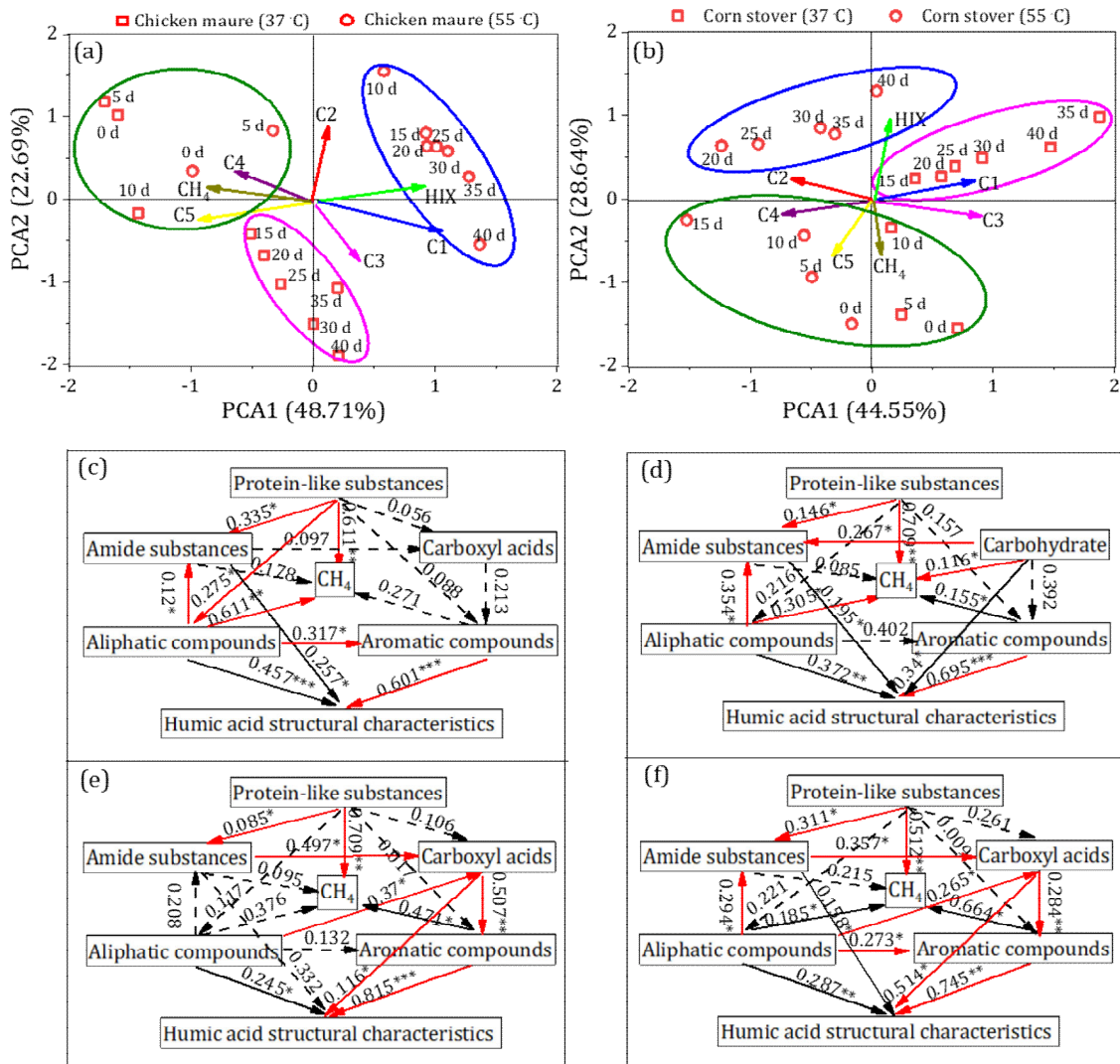
400 3.5 Mechanisms of HA evolution and interaction with CH₄ production

401 PCA and SEM were performed to explore the potential HA evolution pathways in the AD
 402 process with different feeding materials and temperatures (Fig. 5). Three obvious groups
 403 were identified in the PCA coordinates for both the AD of chicken manure (Fig. 5a) and
 404 corn stover (Fig. 5b). For both materials, the samples from the fast CH₄ production stage
 405 were grouped without identifiable differences from the temperature conditions. The
 406 group was located in the up-left area of the coordinate, which was positively contributed
 407 by the PCA component of CH₄ production and negatively contributed by the HIX. It

408 indicates that the humification (HA formation) in the fast CH₄ production stage does not
409 affect CH₄ production. During the slow CH₄ production stage, the samples from the
410 mesophilic and thermophilic AD processes were separated for both materials. Both
411 groups moved towards the down-right area in the coordinates, which were positively
412 contributed by the PCA component of HIX and negatively contribute by the CH₄
413 production. The results represent the significant inhibitory effect of HA on CH₄
414 generation at this stage of the AD process. Moreover, the higher factor contribution of
415 the HIX was observed in the thermophilic AD group, which supported the negative
416 influence of HA on CH₄ production being stronger under thermophilic conditions than
417 under mesophilic conditions. When looking at the HA structures, the results from PCA
418 showed that the protein-like substances (C4 and C5) were negatively correlated with
419 humic-like substances (C1 and C3) and HIX, indicating the potential contribution of the
420 degradation of protein-like substances to HA humification ([Hardie et al., 2009](#); [Zhang et
421 al., 2015](#)).

422 SEM is an effective method to study the complex relationships between latent and
423 observed variables ([Liu et al., 2019](#)), and it has been widely used to interpret and predict
424 interactions in multivariate datasets ([Grace, 2006](#); [Gao et al., 2019](#)). In this study, SEM
425 was used to elucidate the HA evolution along with the organic transformation and CH₄
426 production. The results showed a complex interaction among aliphatic compounds,
427 aromatic compounds, amides, carboxyl acids, and HA structural characteristics (Fig. 5c–
428 f). Generally, in the AD process of chicken manure, amides and aliphatic compounds
429 negatively affect HA structural characteristics but positively influence small molecules,
430 such as carboxyl acids; however, in the AD process of corn stover, carbohydrates and

431 aliphatic compounds have a significantly positive effect on amides, which indirectly
432 influence the HA structural characteristics (Fig. 5d). The contents of amide and aliphatic
433 components in HA have a significantly positive influence on CH₄ production during the
434 fast CH₄ production stage of the chicken manure and corn stover AD processes (Fig. 5c
435 and d). The higher aromatic components in HA have significantly negative impacts on
436 CH₄ production during the later slow CH₄ production stage (Fig. 5e and f). The results
437 indicated that the impact of HA on AD performance significantly depends on the
438 humification degree or aromaticity of HA (Yap et al., 2017; Li et al., 2019a). The aliphatic
439 compounds, amides, and carbohydrates in less humified HA can first be degraded to
440 serve as the carbon resource for microorganisms to produce CH₄ (Tang et al., 2018).
441 When the HA structure becomes more complex and stable with higher aromaticity, an
442 inhibitory effect on CH₄ production may appear (Li et al., 2019b).



443

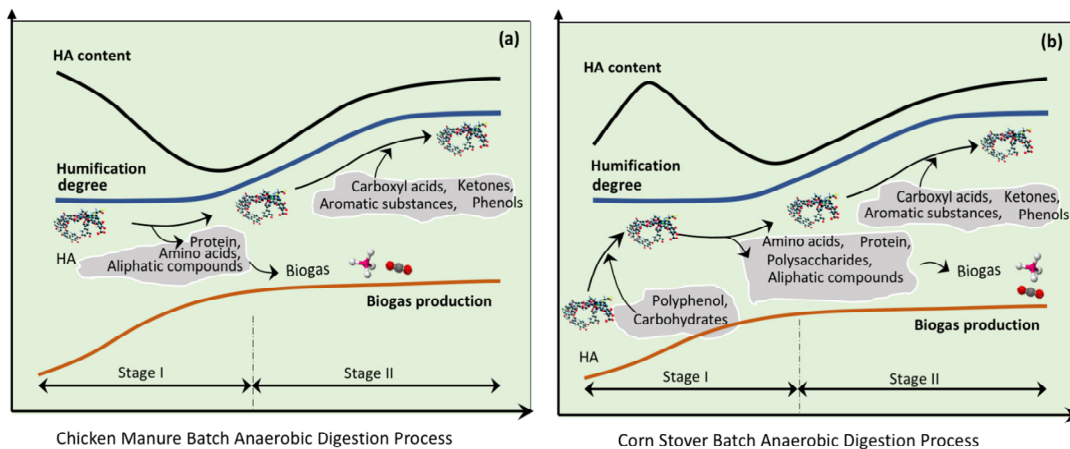
444 **Fig. 5.** Principal component analysis biplot considering the changes in organic matter during the
 445 anaerobic digestion process with (a) chicken manure and (b) corn stover at different
 446 temperatures. A structural equation model (SEM) showing the direct and indirect effects of the
 447 key factors on HA formation and methane production in the fast methane production stage and
 448 slow methane production stage of chicken manure (c), (e) and corn stover (d), (f) anaerobic
 449 digestion. The path coefficients are adjacent to the arrows, *p < 0.05; **p < 0.01; ***p < 0.001.
 450 (HIX: humification index; C1, C3: humic acid-like substance; C2: Fulvic acid-like substance; C4:
 451 Tyrosine-like substance; C5: Tryptophan-like substance)

452

453 To evaluate the possible transformation and decomposition pathways of HA during the
 454 AD process, the species and quantities of HA compositions were assessed in both the
 455 fast and slow CH₄ production stages using Py-GC/MS (Fig. S6). The main compositions of
 456 the HA from the AD of chicken manure and corn stover were slightly different; however,

457 they can be generally categorized into aldehydes, alcohols, amines, acids, ketones,
458 benzenes, phenols, and hydrocarbons (Table S8 and S9). Based on the aforementioned
459 information, the potential mechanism of HA transformation during the AD process is
460 summarized in Fig. 6. In the chicken manure AD process (Fig. 6a), the initial basic
461 structural units of HA, which are composed of a variety of easily degradable substances
462 (such as aliphatic compounds, amides, and protein), were first degraded to contribute
463 to CH₄ production in the fast CH₄ production stage (Tang et al., 2018; Gao et al., 2019).
464 Then, the small molecules, such as those with carboxyl-rich groups of aromatic
465 compounds and amide compounds, attached to these basic units of HA by condensation
466 reactions and finally formed more complex and humified structures (Sánchez-Monedero
467 et al., 1999; Baddi et al., 2009; Said-Pullicino et al., 2016). However, the formation of HA
468 in the corn stover AD process showed different pathways (Fig. 6b). First, the
469 intermediates from carbohydrate and polyphenol compound degradation are rich in
470 carboxyl and hydroxyl moieties and serve as the precursor of HA to form low-molecular-
471 weight compounds with HA characteristics, such as amides. These compounds react
472 with aromatic-like substances to form a tight polymer that is also regarded as the “core”
473 of HA. Then, in a process similar to the chicken manure AD process, easily degradable
474 compounds (such as aliphatic and polysaccharides) were decomposed. As the
475 fermentation continues, some small-molecule organic acids (e.g., carboxyl), as the
476 intermediates between amide and aliphatic compound degradation, attach to the
477 surface of the core of HA, forming more mature and stable HA macromolecules (Jiang
478 et al., 2015; Wu et al., 2017; Gao et al., 2019).

479 CH₄ production was also significantly affected by the dynamic electron transferring
 480 ability of the formed HA, along with their structural evolution during the AD process (Fig.
 481 S7). In the fast CH₄ production stage, the positive effect of HA on CH₄ production may
 482 not only be sacrificing aliphatic compounds, amides, and carbohydrates in HA as carbon
 483 resources, but may also be facilitating the electron transfer chain among various
 484 microbially mediated reactions, such as acidogenesis, acetogenesis, and
 485 methanogenesis (Fernandes et al., 2015; Li et al., 2019a). In the following slow CH₄
 486 production stage, however, the functional groups in more humified HA can bind to the
 487 active sites of relevant key enzymes in AD (such as hydrolytic enzymes), thereby
 488 preventing their access to substrates and resulting in lower CH₄ generation (Yap et al.,
 489 2017). The result also provides evidence that the highly humified HA with high ETC has
 490 the potential to serve as terminal electron acceptors during microbial respiration and to
 491 function as electron shuttles driving the anaerobic oxidation of methane (AOM, Bai et
 492 al., 2019). Note that the microbial community and abundance that perform the HA-
 493 dependent AOM process were not involved in this study; therefore, the direct
 494 relationship between the HA formed by the AD process and the AOM process, functional
 495 microbes, and electron transfer mechanisms needs to be further analyzed.



496

497 **Fig. 6.** The possible transformation and decomposition pathways of humic acid during anaerobic
498 digestion with (a) chicken manure and (b) corn stover.

499 **3.6 Significance of this work**

500 The existence of HA formed in the AD system could create a negative effect on the
501 energy efficiency of the conversion of waste OM to CH₄ (Bai et al., 2019; Li et al., 2019b);
502 however, this conclusion was based on previous studies with the external addition of
503 commercial HA, which can hardly reflect the impact of genuine HA that naturally formed
504 in the AD process with a dynamic structure and function. Our research conducted *in-situ*
505 monitoring of the dynamics of HA evolution, including degradation, formation, structure
506 variation, functional groups, and ETC alternation to re-evaluate the interaction effect.
507 The present study proved that the decomposition of aliphatic, amide, carbohydrate, and
508 protein-like compounds in HA positively correlated with CH₄ production in the fast CH₄
509 production stage, and the accumulation of the re-polymerized HA in the later stage
510 negatively correlated with CH₄ production in the AD process. Moreover, the impact of
511 HA on AD performance is significantly dependent on the humification degree or
512 aromaticity of HA, which varies with fermentation time and temperature. The
513 thermophilic conditions significantly promoted the evolution of the HA structure during
514 the AD process. The formation mechanisms of HA were also different in the AD of
515 different feeding materials, i.e., chicken manure and corn stover. Further studies could
516 investigate the microbial community characterisation in relation to the HA
517 transformation. Nevertheless, with the current results, this study improves our
518 understanding of the transformation of HA itself and its dynamic effects on other carbon
519 metabolism pathways and thus improves the transparency of the knowledge “black box”
520 that exists in the AD process.

521 From the perspective of engineering applications, this study may provide an evidence-
522 based recommendation for optimising the operations of AD process in order to improve
523 the CH₄ production efficiency. The current applied AD plants are normally operated
524 under a hydraulic retention time of 20-30 days for manures (Li et al., 2020) and 40-50
525 days for lignocellulosic biomass (Guo et al., 2018; Xu et al., 2020), respectively.
526 Considering the potential interactive effect of genuine HA formed in the AD process on
527 CH₄ production, the current findings may suggest a shorter retention time. However, to
528 consolidate this conclusion, further research is still needed..

529 **4. Conclusions**

530 This study investigated the evolutionary dynamics of the structure and function of
531 genuine HA that naturally formed in the AD processes and re-evaluated its dynamic
532 interaction with CH₄ production. The concurrent decomposition and re-polymerization
533 of HA during the AD process was observed, however, the HA evolution mechanisms in
534 the AD of chicken manure and corn stover showed different pathways. An accelerating
535 effect of the higher temperature on the evolution of HA through humification was also
536 confirmed from the results of HSQC NMR spectroscopy and 2D-COS-FTIR spectroscopy
537 detections. The HA performed positive and negative effects on CH₄ production in the
538 fast and slow CH₄ production stages, respectively. The dynamic interaction was due to
539 variations in the electron transferring ability and structure of the formed HA. The results
540 could support further research and deployment of AD toward improving AD
541 performance by regulating the evolution of the HA.

542 **Acknowledgments**

543 This work was financed by the AIAS-COFUND fellowship Programme, which is funded by
544 the European Union's Seventh Framework Programme for Research, Technological
545 Development and Demonstration under grant agreement no. 609033.

546 **Appendix A. Supplementary data**

547 Supplementary data associated with this article can be found in the Supporting
548 Information. Text S1–S2, additional analytical methods; Figures S1–S7, daily methane
549 production, the relative proportion of fluorescence components, 2D-COS HSQC NMR
550 spectra, FTIR spectra, ETC, Py-GC/MS spectra, and the relationship between ETC and
551 daily methane production; Table S1–S9, characteristics of physicochemical properties of
552 the AD process, EEM spectra PARAFAC analysis, the percent aliphaticity and aromaticity
553 of HA, elemental composition, SUVA values, and typical products by Py-GC/MS analysis.

554 **References**

- 555 Appels, L., Baeyens, J., Degreve, J., Dewil, R., 2008. Principles and potential of the
556 anaerobic digestion of waste-activated sludge. *Prog. Energ. Combust.* 34, 755-781.
- 557 APHA (American, Public Health Association), AWWA (American Water Works and
558 Protection Association) and WPCF (Water Pollution Control Federation), 1998.
559 Standard Methods for the Examination of Water and Wastewater 20th ed.,
560 Washington, D.C.
- 561 Bahram, M., Bro, R., Stedmon, C., Afkhami, A., 2006. Handling of Rayleigh and Raman
562 scatter for PARAFAC modeling of fluorescence data using interpolation. *J. Chemom.*
563 20, 99-105.
- 564 Bai, Y. N., Wang, X. N., Wu, J., Lu, Y. Z., Fu, L., Zhang, F., Lau, T. C., Zeng, R. J., 2019. Humic
565 substances as electron acceptors for anaerobic oxidation of methane driven by
566 ANME-2d. *Water Res.* 164, 114935.
- 567 Baddi, G.A., Cegarra, J., Merlina, G., Revel, J.C., Hafidi, M., 2009. Qualitative and
568 quantitative evolution of polyphenolic compounds during composting of an olive-
569 mill waste-wheat straw mixture. *J. Hazard. Mater.* 165, 1119–1123.
- 570 Croce, S., Qiao, W., D'Imporzano, G., Dong, R., Adani, F., 2016. Anaerobic digestion of
571 straw and corn stover: The effect of biological process optimization and pre-

572 treatment on total bio-methane yield and energy performance. *Biotech. Advan.* 34,
573 1280-1304.

574 Fernandes, T. V., van Lier, J. B., Zeeman, G., 2015. Humic acid-like and fulvic acid-like
575 inhibition on the hydrolysis of cellulose and tributyrin. *BioEnergy Res.* 8 (2), 821–
576 831.

577 Grace, J. B., 2006. *Structural Equation Modeling and Natural Systems*; Cambridge
578 University Press.

579 Gao, X., Tan, W., Zhao, Y., Wu, J., Sun, Q., Qi, H., Xie, X., Wei, Z., 2019. Diversity in the
580 mechanisms of humin formation during composting with different materials.
581 *Environ. Sci. Technol.* 53, 3653-3662.

582 Guo, X. X., Liu, H. T., Wu, S. B., 2019. Humic substances developed during organic waste
583 composting: Formation mechanisms, structural properties, and agronomic
584 functions. *Sci. Total Environ.* 662, 501-510.

585 Guo, J., Cui, X., Sun, H., Zhao, Q., Wen, X., Pang, C., Dong, R., 2018. Effect of glucose and
586 cellulase addition on wet-storage of excessively wilted maize stover and biogas
587 production, *Bioresour. Technol.* 259, 198-206.

588 He, X. S., Xi, B. D., Gao, R. T., Wang, L., Ma, Y., Cui, D. Y., Tan, W. B., 2015. Using
589 fluorescence spectroscopy coupled with chemometric analysis to investigate the
590 origin, composition, and dynamics of dissolved organic matter in leachate-polluted
591 groundwater. *Environ. Sci. Pollut. Res.* 22, 8499-8506.

592 Hayes, M. H. B., 2009. *Evolution of concepts of environmental natural nonliving organic
593 matter*; Wiley interscience: New York, NY.

594 He, S., Ding, L. L., Li, K., Hu, D. H., Ye, L., Ren, H. Q., 2018. Comparative study of activated
595 sludge with different individual nitrogen compositions, metagenomic and microbial
596 community. *Bioresour. Technol.* 247, 915-923.

597 Huguest, A., Vacher, L., Relexans, S., Saubusse, S., Froidefond, J. M., Parlanti, E., 2009.
598 Properties of fluorescent dissolved organic matter in the Gironde Estuary. *Org.
599 Geochem.* 40(6), 706-719.

600 He, X. S., Xi, B. D., Cui, D. Y., Liu, Y., Tan, W. B., Pan, H. W., Li, D., 2014. Influence of
601 chemical and structural evolution of dissolved organic matter on electron transfer
602 capacity during composting. *J. Hazad. Mat.* 268, 256-263.

603 Hardie, A. G., Dynes, J. J., Kozak, L. M., Huang, P. M., 2009. The role of glucose in abiotic
604 humification pathways as catalyzed by birnessite. *J. Mol. Catal. A Chem.* 308, 114–
605 126.

606 Lopez, M. J., Elorrieta, M. A., Vargas-Garcia, M. C., Suarez-Estrella, F., Moreno, J., 2002.
607 The effect of aeration on the biotransformation of lignocellulosic wastes by white-
608 rot fungi. *Bioresour. Technol.* 81, 123–129.

609 Li, B., Dinkler, K., Zhao, N., Sobhi, M., Merkle, W., Liu, S., Dong, R., Oechsner, H., Guo, J.,
610 2020. Influence of anaerobic digestion on the labile phosphorus in pig, chicken, and
611 dairy manure. *Sci. Total Environ.* 737, 140234.

612 Li, J., Hao, X., van Loosdrecht, M. C. M., Luo, Y., Cao, D., 2019a. Effect of humic acids on
613 batch anaerobic digestion of excess sludge. *Water Res.* 155, 431-443.

614 Li, J., Hao, X., Loosdrecht, M. C. M., Yu, J., Liu, R., 2019b. Adaptation of semi-continuous
615 anaerobic sludge digestion to humic acids. *Water Res.* 161, 329-334.

616 Luo, H., Lyu, T., Muhmood, A., Xue, Y., Wu, H., Meers, E., Dong, R., Wu, S., 2018. Effect
617 of flocculation pre-treatment on membrane nutrient recovery of digested chicken
618 slurry: Mitigating suspended solids and retaining nutrients. *Chem. Eng. J.* 352, 855-
619 862.

620 Liu, Y. R., Yang, Z., Zhou, X., Qu, X., Li, Z., Zhong, H., 2019. Overlooked Role of Putative
621 Non-Hg Methylators in Predicting Methylmercury Production in Paddy Soils.
622 *Environ. Sci. Technol.* 53, 1230-12338.

623 Jiang, J., Liu, X., Huang, Y., Huang, H., 2015. Inoculation with nitrogen turnover bacterial
624 agent appropriately increasing nitrogen and promoting maturity in pig manure
625 composting. *Waste Manag.* 39, 78–85.

626 Ma, S., Hu, H., Wang, J., Liao, K., Ma, H., Ren, H., 2019. The characterization of dissolved
627 organic matter in alkaline fermentation of sewage sludge with different pH for
628 volatile fatty acids production. *Water Res.* 164, 114924.

629 Maynaud, G., Druilhe, G., Daumoin, M., Jimenez, J., Patureau, D., Torrijos, M., Pourcher,
630 A. M., Wery, N., 2017. Characterization of the biodegradability of post-treated
631 digestates via the chemical accessibility and complexity of organic matter.
632 *Bioresour. Technol.* 231, 65-74.

633 Martins des Neves, L. C., Concert, A., Vessoni Penna, T. C., 2009. Biogas production: new
634 trends for alternative energy sources in rural and urban zones. *Chem. Eng. Technol.*
635 32, 1147-1153.

636 Mylotte, R., Sutrisno, A., Farooq, H., Masoom, H., Soong, R., Hayes, M. H. B., Simpson,
637 A. J., 2016. Insight into the composition of recalcitrant organic matter from
638 estuarine sediments using NMR spectroscopy. *Org. Geochem.* 98, 155-165.

639 Noda, I., Ozaki, Y., 2004. Two-dimensional correlation spectroscopy applications in
640 vibrational and optical spectroscopy. John Wiley, England.

641 Nie, X., Li, Z., Huang, J., Liu, L., Xiao, H., Liu, C., Zeng, G., 2018. Thermal stability of organic
642 carbon in soil aggregates as affected by soil erosion and deposition. *Soil Tillage Res.*
643 175, 82-90.

644 Onwosi, C. O., Igbokwe, V. C., Odimba, J. N., Eke, I. E., Nwankwoala, M. O., Iroh, I. N.,
645 Ezeogu, L. I., 2017. Composting technology in waste stabilization: on the methods,
646 challenges and future prospects. *J. Environ. Manag.* 190, 140–157.

- 647 Putranto, A., Chen, X. D., 2017. A new model to predict diffusive self-heating during
648 composting incorporating the reaction engineering approach (REA) framework.
649 *Bioresour. Technol.* 232, 211–221.
- 650 Swift, R. S., Sparks, D. L., Madison, W., 1996. Isolation of IHSS soil fulvic and humic acid
651 from <http://humic-substances.org/isolation-of-ihss-soil-fulvic-and-humic-acids/>.
652 Exerpt from-organic matter characterization (chap 35). In: *Method of soil analysis*,
653 pp. 1018-1020. Part 3. Chemical methods. Soil Sci. Soc. Am. Book Series: 5. Soil Sci.
654 Soc. Am.
- 655 Said-Pullicino, D., Miniotti, E. F., Sodano, M., Bertora, C., Lerda, C., Chiaradia, E. A.,
656 Romani, M., Cesari de Maria, S., Sacco, D., Celi, L., 2016. Linking dissolved organic
657 carbon cycling to organic carbon fluxes in rice paddies under different water
658 management practices. *Plant Soil* 401, 273-290.
- 659 Somers, M. H., Azman, S., Sigurnjak, I., Ghyselbrecht, K., Meers, E., Meesschaert, B.,
660 Appels, L., 2018. Effect of digestate disintegration on anaerobic digestion of organic
661 waste. *Bioresour. Technol.* 268, 568-576.
- 662 Sepehr, S. Y., Hedenstrom, M., Stehr, J. E., Dario, M., Hertkorn, N., Bjorn, A., 2018.
663 Pretreatment of anaerobic digester samples by hydrochloric acid for solution-state
664 ¹H and ¹³C NMR spectroscopic characterization of organic matter. *Chemosphere*,
665 199, 201-209.
- 666 Sánchez-Monedero, M. A., Roig, A., Cegarra, J., Bernal, M. P., 1999. Relationships
667 between water-soluble carbohydrate and phenol fractions and the humification
668 indices of different organic wastes during composting. *Bioresour. Technol.* 70, 193–
669 201.
- 670 Sale, V., Aguilera, P., Laczko, E., Mader, P., Berner, A., Zihlmann, U., van der Heijden, M.
671 G. A., Oehl, F., 2015. Impact of conservation tillage and organic farming on the
672 diversity of arbuscular mycorrhizal fungi. *Soil Biol. Biochem.* 84, 38-52.
- 673 Shahbeig, H., Nosrati, M., 2020. Pyrolysis of biological wastes for bioenergy production:
674 Thermo-kinetic studies with machine-learning method and Py-GC/MS analysis. *Fuel*,
675 269, 117238.
- 676 Tedetti, M., Cuet, P., Guigue, C., Goutx, M., 2011. Characterization of dissolved organic
677 matter in a coral reef ecosystem subjected to anthropogenic pressures using multi-
678 dimensional fluorescence spectroscopy. *Sci. Total Environ.* 409, 2198-2210.
- 679 Tang, Y., Li, X., Dong, B., Huang, J., Wei, Y., Dai, X., Dai, L., 2018. Effect of aromatic
680 repolymerization of humic acid-like fraction on digestate phytotoxicity reduction
681 during high-solid anaerobic digestion for stabilization treatment of sewage sludge.
682 *Water Res.* 143, 436-444.
- 683 Tang, Y., Dai, X., Dong, B., Guo, Y., Dai, L., 2020. Humification in extracellular polymeric
684 substances (EPS) dominates methane release and EPS reconstruction during the
685 sludge stabilization of high-solid anaerobic digestion. *Water Res.* 175, 115686.

686 Tan, K. H., 2014. Humic matter in soil and the environment: Principles and controversies.
687 CRC Press.

688 Tan, W., Xi, B., Wang, G., Jie, J., He, X., Mao, X., Gao, R., Huang, C., Zhang, H., Li, D., Jia,
689 Y., Yuan, Y., Zhao, X., 2017. Increased electron-accepting and decreased electron
690 donating capacities of soil humic substances in response to increasing temperature.
691 Environ. Sci. Technol. 51, 3176–3186.

692 Wu, J. O., Zhao, Y., Zhao, W., Yang, T. X., Zhang, X., Xie, X. Y., Cui, H. Y., Wei, Z. M., 2017.
693 Effect of precursors combined with bacteria communities on the formation of
694 humic substances during different materials composting. Bioresour. Technol. 226,
695 191-199.

696 Weishaar, J. L., Aiken, G. R., Bergamaschi, B. A., Fram, M. S., Fujii, R., Mopper, K., 2003.
697 Evaluation of specific ultraviolet absorbance as an indicator of the chemical
698 composition and reactivity of dissolved organic carbon. Environ. Sci. Technol. 37
699 (20), 4702-4708.

700 Wang, X., Muhmood, A., Dong, R., Wu, S., 2020. Synthesis of humic-like acid from
701 biomass pretreatment liquor: Quantitative appraisal of electron transferring
702 capacity and metal-binding potential. J. Clean. Prod. 255,120243.

703 Wang, M., Zhao, Z., Zhang, Y., 2019. Disposal of Fenton sludge with anaerobic digestion
704 and the roles of humic acids involved in Fenton sludge, Water Res. 163, 114900.

705 Xu, H., Li, Y., Hua, D., Zhao, Y., Mu, H., Chen, H., Chen, G. 2020. Enhancing the anaerobic
706 digestion of corn stover by chemical pretreatment with the black liquor from the
707 paper industry. Bioresour. Technol. 306, 123090.

708 Yap, S. D., Astals, S., Lu, Y., Peces, M., Jensen, P. D., Batstone, D. J., Tait, S., 2018. Humic
709 acid inhibition of hydrolysis and methanogenesis with different anaerobic inocula.
710 Waste Manage. 80, 130-136.

711 Yap, S. D., Astals, S., Jensen, P. D., Batstone, D. J., Tait, S., 2017. Indigenous microbial
712 capability in solid manure residues to start-up solid-phase anaerobic digesters.
713 Waste Manage. 64, 79-87.

714 Yang, F., Zhang, S., Cheng, K., Antonietti, M., 2019. A hydrothermal process to turn waste
715 biomass into artificial fulvic and humic acids for soil remediation. Sci. Total Environ.
716 686, 1140-1151.

717 Zhang, W., Wei, Q., Wu, S., Qi, D., Li, W., Zuo, Z., Dong, R., 2014. Batch anaerobic co-
718 digestion of pig manure with dewatered sewage sludge under mesophilic
719 conditions. Appl. Energ. 128, 175-183.

720 Zhao, X., Tan, W., Peng, J., Dang, Q., Zhang, H., Xi, B., 2020. Biowaste-source-dependent
721 synthetic pathways of redox functional groups within humic acids favoring
722 pentachlorophenol dichlorination in composting process. Environ. Intern. 135,
723 105380.

- 724 Zhou, Y., Selvam, A., Wong, J. W. C., 2014. Evaluation of humic substances during co-
725 composting of food waste, sawdust and Chinese medicinal herbal residues.
726 *Bioresour. Technol.* 168, 229-234.
- 727 Zhang, Y. C., Yue, B. D., Ma, H., 2015. Darkening mechanism and kinetics of humification
728 process in catechol-Maillard system. *Chemosphere*, 130, 40–45.
729